Chemical Trends in Solid Alkali Pertechnetates

Jamie Weaver,[†,‡] Chuck Z. Soderquist,[‡] Nancy M. Washton,[‡] Andrew S. Lipton,[‡] Paul L. Gassman,[‡] Wayne W. Lukens,[§] Albert A. Kruger,[∥] Nathalie A. Wall,[†] and John S. McCloy*,[†,‡,⊥]

[†]Department of Chemistry, Washington State University, Pullman, Washington 99164, United States
[‡]Pacific Northwest National Laboratory, Richland, Washington 99352, United States
[§]Lawrence Berkeley National Laboratory, Berkeley, California 94720, United States
[∥]U.S. Department of Energy (DOE), Office of River Protection, Richland, Washington 99352, United States
[⊥]Materials Science and Engineering Program and School of Mechanical & Materials Engineering, Washington State University, Pullman, Washington 99164, United States

S *Supporting Information*
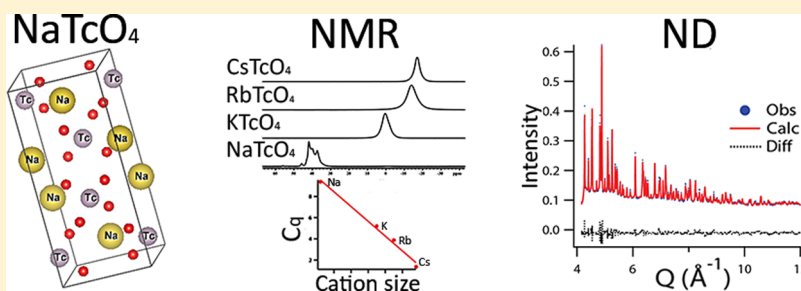
ABSTRACT: Insight into the solid-state chemistry of pure technetium-99 (^{99}Tc) oxides is required in the development of a robust immobilization and disposal system for nuclear waste stemming from the radiopharmaceutical industry, from the production of nuclear weapons, and from spent nuclear fuel. However, because of its radiotoxicity and the subsequent requirement of special facilities and handling procedures for research, only a few studies have been completed, many of which are over 20 years old. In this study, we report the synthesis of pure alkali pertechnetates (sodium, potassium, rubidium, and cesium) and analysis of these compounds by Raman spectroscopy, X-ray absorption spectroscopy (XANES and EXAFS), solid-state nuclear magnetic resonance (static and magic angle spinning), and neutron diffraction. The structures and spectral signatures of these compounds will aid in refining the understanding of ^{99}Tc incorporation into and release from nuclear waste glasses. NaTcO$_4$ shows aspects of the relatively higher electronegativity of the Na atom, resulting in large distortions of the pertechnetate tetrahedron and deshielding of the ^{99}Tc nucleus relative to the aqueous TcO$_4^-$. At the other extreme, the large Cs and Rb atoms interact only weakly with the pertechnetate, have closer to perfect tetrahedral symmetry at the Tc atom, and have very similar vibrational spectra, even though the crystal structure of CsTcO$_4$ is orthorhombic while that of RbTcO$_4$ is tetragonal. Further trends are observed in the cell volume and quadrupolar coupling constant.

1. INTRODUCTION

Technetium (Tc, element 43) was first isolated in 1937 by the Italian researchers Perrier and Segre from molybdenum foil that had been bombarded with deuterons. Since its discovery, it has been found to have uses in the medical industry (~85% of all radionuclear scans in the U.S. utilize short-lived ^{99m}Tc[1]), in the steel industry as a corrosion inhibitor,[2] and as a low-temperature superconductor.[3] Additionally, identification of Tc in the spectrum of a variety of star types leads to new research in the solar production of heavy elements.[4,5] From the standpoint of inorganic chemistry, the research completed on the element since the late 1930s has worked to fill in the gaps of understanding the periodic trends for transitions metals, particularly those related to the formation of chromium and rhenium oxyanions.[6]

Of its 21 isotopes (mass numbers 90−111), all of which are radioactive, ^{99}Tc is the most common and abundant, and because of its high mobility under oxidizing conditions in the subsurface environment and long half-life ($t_{1/2} = 2.11 \times 10^5$ years), ^{99}Tc is considered to be a significant environmental hazard.[1,2] ^{99}Tc is common on earth today because it is a byproduct of the fission of uranium and plutonium in nuclear reactors: 6.1% and 5.9% mass yields, respectively. It is the only long-lived Tc isotope produced on a gram scale by this pathway. It is also the daughter product in the decay of ^{99m}Tc. For long-term nuclear waste management, ^{99}Tc is the dominant producer of radiation in the period from about 10^4-10^6 years, in becquerels (Bq) per mass of spent fuel. Because of its

radiotoxicity (^{99}Tc is a soft β emitter, 292 keV), high environmental mobility, and long half-life, its immobilization and safe long-term storage is a priority goal to countries that are in the process of disposing of nuclear waste. A current challenge to efficient immobilization of the radioisotope can be linked to a lack of understanding of the behavior of Tc during vitrification, the process of turning nuclear waste into glass, and it localized chemistry in waste glasses.

One cause of this deficit is the dearth of recent published characterization data on relevant pure Tc compounds, particularly alkali technetium oxides. Alkali pertechnetate solid-state chemistry is of particular importance because investigations into the oxidation state and chemistry of Tc during low-activity-waste (LAW) vitrification showed that Tc^{VII}, probably in the form of alkali pertechnetates, is the major Tc oxidation state throughout the expected waste management processes.[7,8] Raman studies of glasses with a typical LAW composition containing low concentrations of Tc have shown that the local structures of Tc under these conditions resemble KTcO$_4$, NaTcO$_4$, or an isolated pertechnetate anion, TcO$_4^-$.[9,10] One challenge in the incorporation of Tc^{VII} into glass melt is its high volatility at vitrification temperatures.[11,12] The mechanism by which this volatility occurs is still not well understood; however, Tc will volatilize at a greater rate if significant Cs is present and may be related to the chemistry of CsTcO$_4$.[13] Another important application of alkali pertechnetates is the use of KTcO$_4$ as a common starting material in the synthesis of Tc-based radiopharmaceuticals.

Because of its radiotoxicity and requisite handling procedures, only a few studies, many of which are more than 20 years old, have been reported for alkali pertechnetates, and even fewer have investigated the periodic trends of solid alkali pertechnetates.[14–16] The study here rectifies this gap in the literature by presenting a modern investigation of the structure and localized chemistry of solid sodium, potassium, rubidiun, and cesium pertechnetates, using state-of-the-art X-ray absorption spectroscopy (XAS), including Tc K-edge X-ray absorption near-edge spectroscopy (XANES) and extended X-ray absorption fine structure (EXAFS) analysis, neutron diffraction (ND), high-resolution Raman spectroscopy, and ^{99}Tc solid-state nuclear magnetic resonance (NMR).

2. BACKGROUND

Although the oxidation states of Tc can vary from 7+ to 1−, much of the research has been conducted on stable Tc^{VII} compounds.[6] Most of those publications have focused on the chemistry of pertechnetates in solution, while less research has focused on solid pertechnetate salts. KTcO$_4$ has been the most commonly studied solid alkali pertechnetate. The predominance of data on this salt appears to be related to the fact that it is easily formed by ion-exchange methods, is often used as a starting material for radiopharmaceuticals, and does not readily form a hydrated complex when exposed to the atmosphere.[6,17,18] The latter is not true for NaTcO$_4$, which has three reported hydrated forms, NaTcO$_4$·H$_2$O, NaTcO$_4$·2H$_2$O, and NaTcO$_4$·4H$_2$O, although little data are available on their structural differences.[19] Because of its lack of utility in the nuclear medicine industry, RbTcO$_4$ has been mostly ignored in the literature except when studied within the context of the other alkali pertechnetates.[14,20] CsTcO$_4$ has received more attention, with an increase in research on the material in recent years because of its link to the volatility of Tc during

vitrification.[12,21] Both NMR and X-ray diffraction (XRD) data have been reported for CsTcO$_4$.[12,22,23]

Rhenium (Re) has commonly been used in the place of Tc because of the safety concerns surrounding the handling of radioactive material and because it has similar chemistry in a given oxidation state, as Re is below Tc on the periodic table.[6,24] However, the standard reduction potential of Tc^{VII} is greater than that of Re^{VII}.[25] Additionally, work by a number of researchers has shown significant dissimilarities between the speciation and incorporation of Re and Tc in nuclear waste glass.[8,10,26–28] In this study, Re analogues of all alkali pertechnetates were prepared to establish protocols for the synthesis of Tc compounds. However, no further discussion will be made regarding their chemistry in this current work, other than as a comparison, because alkali perrhenates have been much more extensively studied than the corresponding pertechnetates.

3. EXPERIMENTAL SECTION

3.1. Synthesis. Tc was obtained from the U.S. DOE Isotopes Program, Oak Ridge National Laboratory (ORNL), Oak Ridge, TN. As received, Tc was in the form of solid NH$_4$TcO$_4$, black and badly decomposed from its own β radiation. The as-received material (approximately 10 g) was transferred to a 125 mL glass Erlenmeyer flask. All chemicals used in this work, except ^{99}Tc, were analytical reagent grade. Water was taken from a Millipore deionizer, 18 MΩ cm or higher resistivity. Approximately 50 mL of concentrated NH$_4$OH and several milliliters of 30% H$_2$O$_2$ were added. The mixture was stirred with a magnetic stir bar and gently warmed, with a small glass funnel serving as a spray trap on the top of the flask. NH$_4$TcO$_4$ dissolved in a few minutes to give a colorless solution of NH$_4$TcO$_4$. The solution was warmed at near boiling for 1 h to decompose H$_2$O$_2$, and then the spray trap was removed to allow the water and NH$_4$OH to evaporate. After nearly all of the water had evaporated, fine crystalline NH$_4$TcO$_4$ was centrifuged out of the solution, washed with dry ethanol to remove water, and then dried to a constant weight at ~90 °C.

Ammonium pertechnetate was converted into aqueous HTcO$_4$ by cation exchange. Crystalline ammonium pertechnetate was dissolved in water and then passed through a column of hydrogen-form cation resin (Dowex 50W-X8, 50−100 mesh, 15 mL resin volume, in water). This volume of resin has a cation capacity of about 1.8 g of NH$_4$TcO$_4$, loaded to 50% of theoretical capacity. By loading to only 50% of the cation capacity of the resin, no cations break through the column to contaminate the pertechnic acid. The cation column effluent was periodically checked with pH strips to confirm that the effluent was always acidic. The column effluent was transferred to a 125 mL round-bottom flask. The solution was stirred and heated, while dry nitrogen gas was gently blown over the surface of the solution to evaporate the water. The nitrogen gas quickly evaporated the water and kept the temperature low enough to avoid bubbles breaking at the surface, even with the heat set high, so that no spray from bursting bubbles could carry Tc out of the flask. This apparatus permits dilute pertechnic acid to be safely evaporated and concentrated without causing airborne β contamination in the fume hood.

Sodium pertechnetate was prepared by neutralizing aqueous HTcO$_4$ with aqueous NaOH to pH 7. The product NaTcO$_4$ solution was then evaporated under flowing nitrogen in a 125 mL round-bottom flask, with heat and stirring, until only wet-crystalline NaTcO$_4$ remained in the flask. The solid NaTcO$_4$ was dried to a constant weight at 120 °C to make the anhydrous salt. Potassium pertechnetate was prepared in the same way, using KOH. Cesium and rubidium pertechnetates were prepared by combining stoichiometric amounts of Rb$_2$CO$_3$ and Cs$_2$CO$_3$, weighed as dry solids, with accurately weighed amounts of NH$_4$TcO$_4$ dissolved in water. The product solutions of RbTcO$_4$ and CsTcO$_4$ were evaporated to expel water and ammonium carbonate. When the volume was 2−3 mL, the crystalline products were

Table 1. Lattice Parameters: Literature and Determined from Neutron Scattering[a]

	a (Å)	b (Å)	c (Å)	unit cell volume (Å³)[b]	cryst syst	thermal parameter (U_{iso})[b]		space group	ref	CIF
NaTcO₄	5.342(3)		11.874(6)	338.91(1)	tetragonal	Na	0.01398(7)	I4₁/a	b	SI
	5.339(1)		11.869(5)			Tc	0.0280(5)		31	no
	5.337(2)		11.88(2)			O	0.01318(2)		60	no
KTcO₄	5.647(4)		12.909(9)	411.73(2)	tetragonal	K	0.01144(2)	I4₁/a	b	SI
	5.654		13.030			Tc	0.01664(3)		36, 81	no
	5.630(2)		12.87(2)			O	0.0262(8)		60	no
	5.630		12.867						16, 20	yes
RbTcO₄	5.762(0)		13.543(5)	449.65(3)	tetragonal	Rb	0.01115(1)	I4₁/a	b	SI
	5.758(2)		13.54(2)			Tc	0.01967(5)		20, 60, 80	yes
						O	0.02971(12)			
CsTcO₄	5.727(1)	5.921(8)	14.341(1)	486.38(3)	orthorhombic	Cs1	0.02293(3)	Pnma	b	SI
	5.718	5.918	14.304			Cs2	0.0137(3)		36	yes
	5.726(2)	5.922(2)	14.36(2)			Tc	0.03535(4)		60	no
	5.72(7)	5.92(1)	14.34			O1	0.03251(3)		22	yes
	5.726	5.922	14.34			O2	0.0484(14)		82	yes
	5.898		14.38		tetragonal	O3	0.0422(9)	not stat.	43	no

[a]Parentheses are ± in the last decimal place listed. [b]Denotes this current work.

centrifuged out of solution and then dried to a constant weight at 120 °C.

3.2. Diffraction. Neutron scattering experiments were performed at the Nanoscale-Ordered Materials Diffractometer (NOMAD) at the Spallation Neutron Source (SNS) at ORNL.[29] Powdered samples (200−400 mg) were flame-sealed in fused-quartz thick-walled (~1 mm wall thickness) NMR tubes to prevent a dispersibility of >1 mCi (>37 MBq) of each powder. ND data were collected over a Q range of 0.04−50 Å⁻¹ at room temperature. The total duration of the data collection for each sample was ~10 h, taken in ~20 min intervals and summed at the end to better reduce noise.

ND was carried out on alkali pertechnetates to verify the identity of each material and to develop modern experimental crystallographic information files (CIFs) for each compound (see the Supporting Information, SI). A comparison of the acquired ND patterns against previously published CIFs for some of the pertechnetates, obtained by other means, showed that the synthesized materials were the expected alkali pertechnetates. Rietveld refinements of the structures were completed, and the χ^2 value calculated for each fit was <25. The larger χ^2 value for some samples was most likely the result of low sample masses in the analysis tubes and therefore a small signal-to-background ratio in the final data sets.

Refinements of alkali pertechnetate diffraction patterns were performed in General Structure Analysis System (GSAS) using EXPGUI[30] starting with the lattice parameters and positions of previously reported structures (listed in Table 1). Refinements were also checked in TOPAS (Bruker), and similar results were obtained. Bond lengths and angles were calculated using the DISAGL routine in GSAS, and thermal parameters were fit using the U_{iso} subroutine. For NaTcO₄, the alkali atom and starting O positions were assumed to be the same as those reported for KTcO₄.[16,31] The coordinates and thermal parameters of atoms not on special positions were allowed to vary during refinement. Similar methods were used in the refinement of other alkali pertechnetates.

To further verify the identity of the materials, each sample was analyzed by capillary XRD. Specimens for powder XRD were sealed in thin-walled glass capillaries (500 μm diameter and 10 μm wall thickness; Charles Supper Co., Natick, MA), which, in turn, were contained in a tight-fitting Kapton sleeve and sealed at both ends with quick-setting epoxy inside as a secondary protection against the spread of radiological material. A Rigaku D/Max Rapid II microdiffraction system with a rotating Cr target (λ = 2.2910 Å) operated at 35 kV and 25 mA was used to collect the diffraction patterns. A parallel X-ray beam collimated to 300 μm diameter was directed onto the specimen, and the diffracted intensities were recorded on a large two-dimensional

(2D) image plate exposed for 5 min. The 2D images were integrated between 2θ = 5 and 160° to give powder traces (see the SI).

3.3. XAS. XAS data were obtained at the Stanford Synchrotron Radiation Lightsource (SSRL) beamline 11-2 at room temperature. X-rays were monochromatized using a double-crystal monochromator with Si(220) crystals, with the second crystal being detuned by 50% to reduce the harmonic content of the beam. The monochromator was energy-calibrated to 21059 eV using the half-height of the Tc K-edge of TcO₄⁻ adsorbed on an ion-exchange resin. The incident and transmitted beam intensities were measured using argon-filled ionization chambers. EXAFS data were obtained on all compounds in transmission mode.

Data were averaged using the software package SixPack.[32] EXAFS data were fit using the programs ATHENA and ARTEMIS using theoretical scattering curves calculated using FEFF 8.5 and the atomic positions of K, Tc, and O in crystalline KTcO₄.[33] The value of S_0^2 was determine to be 0.8 by fitting the EXAFS spectra of several spectra of the energy reference, TcO₄⁻ adsorbed on an ion-exchange resin. For the sodium, rubidium, and cesium pertechnetates, K was replaced by the corresponding alkali metal in the FEFF 8.5 calculation. The value of reduced χ^2 was used as the criterion to determine which model was best.

XANES calculations were performed using FEFF 10.0 and atomic positions from the crystal structures of each alkali pertechnetate or the crystal structure of the analogous alkali perrhenate with Tc substituted for Re. The local density of states (DOS) plots were convolved with a 2 eV Lorentzian function to account for the resolution of the experimental spectra.

3.4. Raman Spectroscopy. Alkali pertechnetates were analyzed using a Horiba high-resolution confocal inverted-stage microscopic Raman spectrometer (LabRam HR8000) with a 1800 grooves/mm diffraction grating, using a Nikon Eclipse Ti microscope. Laser excitation at 532 nm was provided by a Quantum Laser MPC-3000, which delivered ~20 mW of power to samples with an approximate spot diameter of 1 μm on the samples. Spectra were recorded using a Peltier-cooled Horiba Synapse charge-coupled-device detector with a 1024 × 256 pixel array. The spectrometer was calibrated using the line positions of a Hg pen lamp, and the band position of an amorphous Si wafer was used for frequency verification. The spectral resolution of the system, as described, was 1.8 cm⁻¹/pixel with a laser spot size of 1.1 μm. The spectrometer position was 950 cm⁻¹, allowing data collection from 1750 to ~50 cm⁻¹. The number of spectral acquisitions, count times, and diameter of the confocal iris were varied to maximize the signal-to-noise ratio of spectra for each sample. These highly crystalline alkali pertechnetates only required 2–10 s of acquisition time to achieve very strong signal-to-noise ratios and did
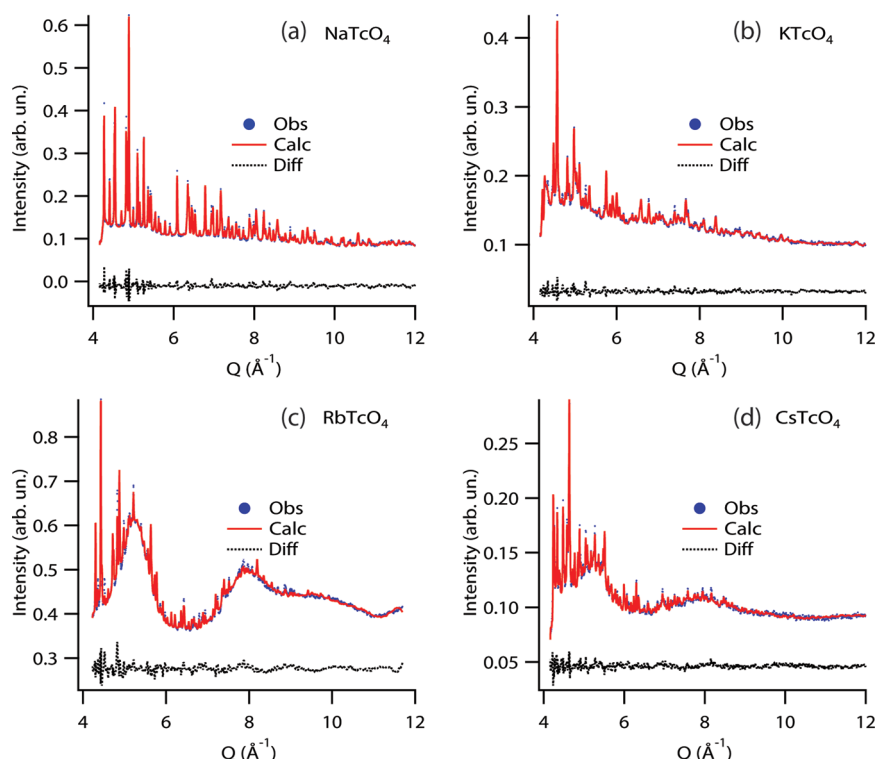
Figure 1. ND spectra and fits of the alkali pertechnetates (a) $NaTcO_4$, (b) $KTcO_4$, (c) $RbTcO_4$, and (d) $CsTcO_4$.

Table 2. Refined Bond Lengths and Angles from ND Data, As Determined by *DISAGL* in *GSAS*, and Goodness-of-Fit Parameters

compound	starting CIF for refinement	Tc−O bond length (Å)	O−Tc−O angle (deg)	alkali−O bond length (Å)	χ^2
$NaTcO_4$	16, 31	1.737(4)	108.03(14), 112.4(3)	2.533(5), 2.7625(14)	20.160
$KTcO_4$	16, 20	1.739(14)	108.05(8), 110.19(14)	2.8936(17), 2.86(8)	21.530
$RbTcO_4$	60[a]	1.723(3)	108.34(9), 110.04(14)	3.021(3), 2.901(3)	1.210
$CsTcO_4$	82	1.640(11),[b] 1.700(5)[b]	112.9(5), 108.6(3), 110.5(5), 108.11(17)	3.071(13), 3.169(7), 3.323(6), 3.645(6),[c] 3.118(12), 3.776(6), 3.645(9), 3.151(13),[c] 3.176(12),[c] 3.287(3),[c] 3.201(11)[c]	4.840

[a]Refinement for $RbTcO_4$ was performed with a starting CIF from ref 60 as cited in refs 80 and 20. [b]The sample had a large background, so errors are higher than expected. [c]Cs−O bond for the second Cs species in the structure.

not require any spectral manipulation to provide very strong and well-resolved Raman bands. On some occasions, it was observed that the mode intensities varied as a function of laser location on the sample. It is assumed that this is due to the various crystallographic orientations and geometry of the experiment.

3.5. NMR Spectroscopy. Solid-state ^{99}Tc NMR spectra were acquired at ambient temperature in a wide-bore (89 mm) Bruker Biospin Ultrashield magnet operating at 16.6 T (750 MHz for ^1H and 168.89 MHz for ^{99}Tc) utilizing an AVANCE III spectrometer with a home-built 3.2 mm HX MAS probe (double tuned at ^1H and ^{99}Tc). Chemical shifts were referenced to external aqueous 0.10 M TcO_4^- (0.0 ppm). Solid samples of approximately 75 μg of powdered alkali pertechnetate (~100 μCi or 3.7 MBq) were packed into specially designed Torlon inserts that were sealed and placed inside commercial 3.2 mm PENCIL style (Agilent or Revolution NMR) zirconia NMR rotors. Magic-angle-spinning (MAS) spectra were collected with selective radio-frequency (RF) pulses of 37 kHz (1.35 μs selective $\pi/2$), a spin rate of 18 kHz, and a recycle time of 1.5 s. Static spectra were obtained utilizing a spin-echo sequence ($\pi/2 - \tau - \pi/2 - \tau$) with τ values of 50 and 1 μs selective $\pi/2$ pulses (50 kHz RF). The ^{99}Tc spectra were analyzed using finite pulse simulations with the *SIMPSON* program.[34]

4. RESULTS AND DISCUSSION

4.1. Crystallography. Figure 1 shows the data (blue) and fits (red) for the ND experiments. Lattice parameters of refined structures are shown in Table 1 and compare well to the literature; corresponding perrhenate lattice parameters can be found elsewhere.[35] One Tc−O bond length was found for sodium, potassium, and rubidium pertechnetate, while two Tc−O bond lengths were found for cesium pertechnetate. These results are consistent with the predicted structures for the compounds: scheelite $I4_1/a$ for sodium, potassium, and rubidium pertechnetate and pseudoscheelite $Pnma$ for cesium pertechnetate.[16,36−38] Two O−Tc−O bond angles were calculated for sodium, potassium, and rubidium pertechnetates, while four different angles were calculated for $CsTcO_4$. These data are shown in Table 2 and the corresponding CIFs are available in the SI. Among the isostructural sodium, potassium, and rubidium pertechnetates, the lengths of the Tc−O bonds are nearly identical; however, the deviation of ∠O−Tc−O from an ideal tetrahedral complex is much greater in $NaTcO_4$ (deviation of 1.5 and 2.9°) than in $KTcO_4$ (1.5 and 0.7°) or $RbTcO_4$ (1.2 and 0.5°).
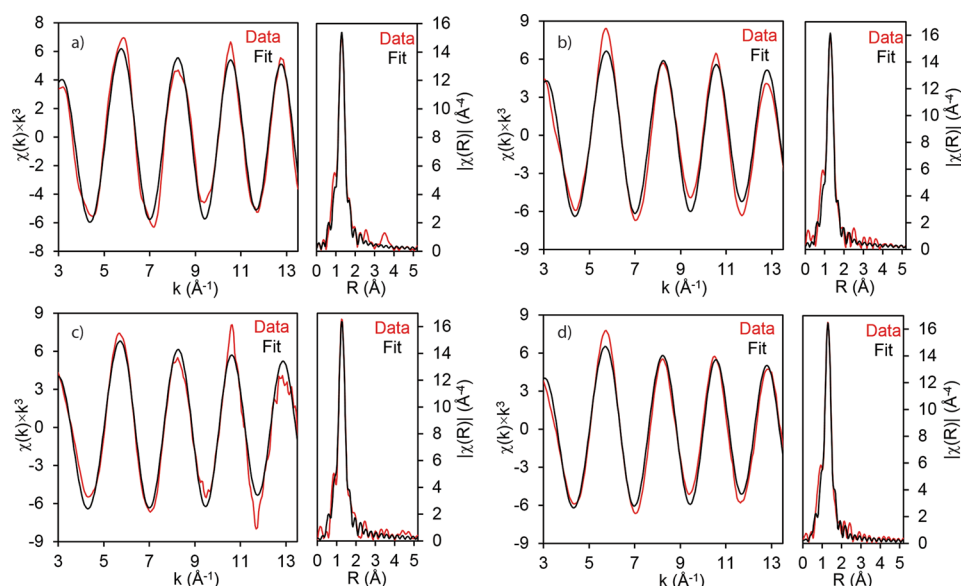
Figure 2. Data (red line) and fits (black line) from Tc K-edge EXAFS of (a) $NaTcO_4$, (b) $KTcO_4$, (c) $RbTcO_4$, and (d) $CsTcO_4$.

4.2. EXAFS. All EXAFS spectra of the alkali pertechnetates are best modeled with a single Tc−O distance of ∼1.73 Å, which is typical of pertechnetates.[39] The EXAFS data as well as calculated fits for all of the alkali pertechnetates can be seen in Figure 2. The data were consistent with the presence of only the $TcO_4^−$ anion and support only a single Tc−O scattering path. Including additional scattering paths increased the value of the reduced χ^2 for all compounds. The Tc−O bond distances determined by EXAFS were within the error of the bond distances determined by ND, and bond length differences are expected as a result of the different methods, where EXAFS measures the local structure interatomic spacing while diffraction measures the average interplanar spacing, and any disordering causes divergence of the two values.[40,41] For $NaTcO_4$, the number of nearest neighbors is slightly lower than the expected value of 4.0, and the value of the Debye−Waller factor (σ^2) was also lower than that for the other compounds; nevertheless, the number of nearest O neighbors was within 2 standard deviations from the expected value of 4.0. The best-fit parameters for all materials are reported in Table 3, with additional information provided in Table S-5.

Table 3. Best-Fit Tc K-Edge EXAFS Parameters for Alkali Pertechnetate Salts (*FEFF 8.5*)

compound	neighboring atom	no. of neighboring atoms	σ^2 ($Å^2$)	Tc−O distance (Å)
$NaTcO_4$	O	3.6(2)	0.0007(3)	1.731(3)
$KTcO_4$	O	4.1(2)	0.0010(3)	1.736(3)
$RbTcO_4$	O	4.3(3)	0.0011(5)	1.713(5)
$CsTcO_4$	O	4.1(2)	0.0011(3)	1.723(5)

4.3. XANES. XANES spectra were aligned to $^1/_2$ the height energy of the edge feature using the reference spectrum of $TcO_4^−$ adsorbed onto an ion-exchange resin. A stack plot of the spectra is shown in Figure 3. There are two main regions of the spectra. At the low-energy side of the edge, several bound state transitions (1s to empty d, s, p, and f orbitals) form the rising part of the edge. To slightly higher energy (∼21060 eV) is the actual edge where the 1s electron is photoionized and no longer
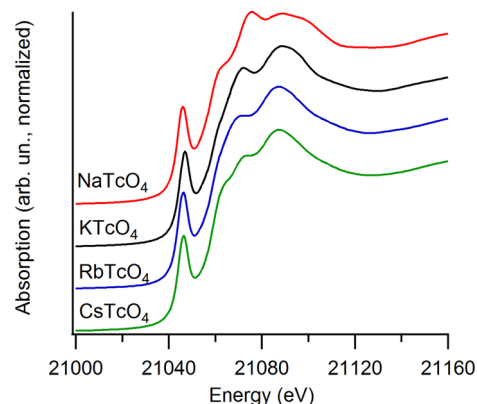

Figure 3. XANES spectra of pertechnetates, offset for clarity.

bound. The lowest-energy transition is the 1s to 4d transition, the symmetry of which is forbidden if an inversion center is present. Here the transition is somewhat allowed because of the lack of an inversion center in the tetrahedral $TcO_4^−$ anion. For all compounds, the 1s to 4d transition is equally intense; therefore, no significant fraction of Tc in these samples has an inversion center. These results are consistent with EXAFS analysis.

The XANES spectra of these compounds have been deconvolved by fitting them to a series of pseudo-Voigt peaks and an arctan function (edge transition). This method has not been previously reported in the literature, so a more detailed description of the process is provided herein. The peaks are tentatively assigned by comparison with the spectra calculated using *FEFF 10* (Figure 4). These plots show the DOSs for the s, p, d, and f orbitals (sDOS, pDOS, dDOS, and fDOS) of Tc. As noted above, the sharp peak at low energy is the 1s to 4d transition. The other peaks are due to the 6s/5p and 4f final states in order of increasing energy. For the alkali pertechnetates, the position and area of the 4d peak is not strongly affected by the identity of the alkali cation. However, the energies and areas of the other peaks change as the identity of the cation changes. This is possibly due to changes in the distance between the cation and anion and the orientation of
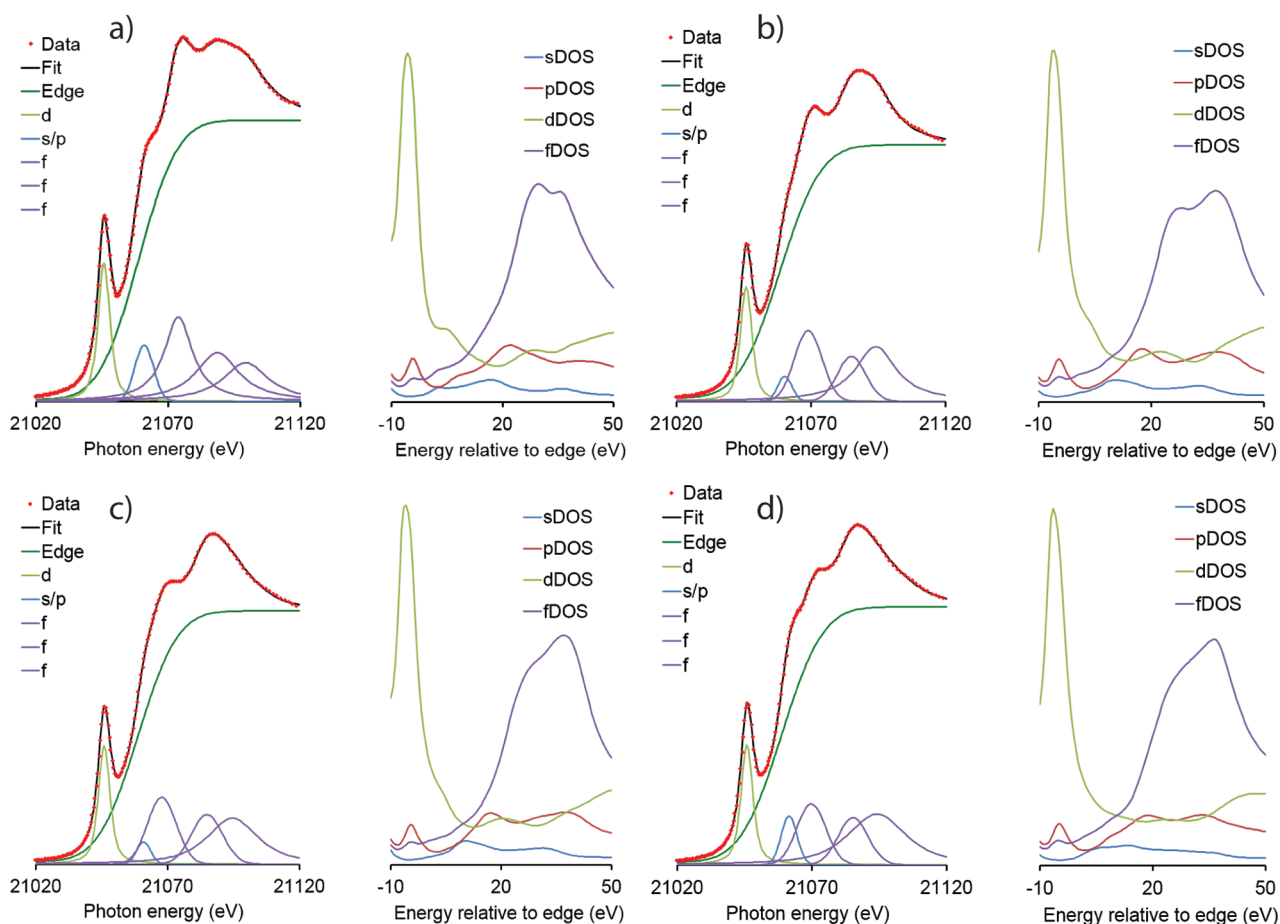
Figure 4. Tc K-edge XANES spectrum and fit for all of the alkali pertechnetates and their calculated DOS (right of each spectrum): (a) $NaTcO_4$; (b) $KTcO_4$; (c) $RbTcO_4$; (d) $CsTcO_4$.

the cations with respect to the pertechnetate anion. The changes appear to be systematic. The intensity and energy of the sharp, low-energy 4f final site decrease as one progresses from Na to Cs. These changes allow the edge structure to be used as a fingerprint for the local environment of TcO_4^-. The XANES spectra reflect both the presence of the tetrahedral TcO_4^- anion (the 1s to 4d peak is equally intense in all samples), and the identities and locations of the cations relative to the TcO_4^- anion (changes in the 1s to 4f transitions). Thus, the XANES spectra can be used as fingerprints to indicate the presence of a specific crystalline phase.

4.4. Raman. The Raman spectra of the alkali pertechnetates exhibit sharp bands, characteristic of crystalline salt species (Figure 5). Sodium, potassium, and rubidium pertechnetates are all tetragonal and possess a scheelite structure ($CaWO_4$) with space group $I4_1/a$.[16,19,31,37] The Tc atom is on a site with $\bar{4}$ symmetry (point group S_4). $CsTcO_4$ has been reported as either being tetragonal or orthorhombic.[22,23,42,43] ND analysis with Rietveld refinement as well as XRD of $CsTcO_4$ synthesized for this study supports the orthorhombic assignment of the structure, but refined χ^2 for the ND spectrum is not as good as the other samples (see Table 2). The space group for $CsTcO_4$ prepared by low-temperature synthesis is $Pnma$, and it is isostructural with $CsIO_4$ and $CsReO_4$.[6,44−50] The Tc atom occupies a site with only mirror symmetry (point group C_s). A correlation diagram illustrating the mode derivations for $I4_1/a$ scheelite[10] and $Pnma$ pseudoscheelite[51−53] structures can be found elsewhere.
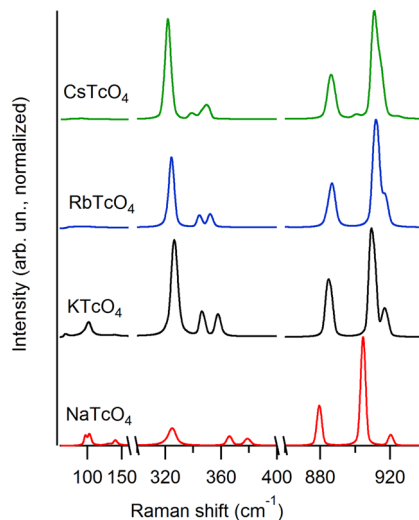

Figure 5. High-resolution Raman spectra (1600 grooves/mm) of alkali pertechnetate salts.

The Raman spectrum of $NaTcO_4$ is in good agreement with the spectrum that was recently published.[10] Similarly, the spectrum for $KTcO_4$ is in agreement with previously published spectra.[10,15] There is only one known published low-resolution Raman spectrum for rubidium and cesium pertechnetate.[53] The band positions for these two materials are very similar despite the different site symmetries of the TcO_4^- ions. No evidence

for structural water modes of ~3000 cm^{-1} was seen in any sample, including NaTcO$_4$. Because RbTcO$_4$ is isostructural to KTcO$_4$ and NaTcO$_4$, it is assumed that the mode assignments for the Rb compound are like those for the Na and K compounds, while the same cannot be argued for CsTcO$_4$. Mode assignments for this compound must be made based on a comparison to the low-temperature and -pressure Raman spectra of orthorhombic CsIO$_4$[44,45] and β-CsReO$_4$.[46] However, it is observed that the spectra for RbTcO$_4$ and CsTcO$_4$ are very similar, despite having different crystal structures. It can be assumed that the countercation size has a lesser effect on the Tc tetrahedral vibrational modes as the cation size increases, and it has been stated that, as the cation size increases, the degree of tetrahedral distortion around the Tc atom decreases.[14,53] If this is the case, the extremes of large cations should have very symmetrical TcO$_4$ tetrahedra and thus similar vibrational modes in the Raman spectra, as observed in RbTcO$_4$ and CsTcO$_4$. Individual spectra with labeled peaks and a summary of the mode frequencies are supplied in Table S-6.

The most notable trend among the compounds is the energy of the symmetric stretch (ν$_3$) of the isostructural compounds, which decreases with a decrease of the alkali cation radius from 912 cm^{-1} in RbTcO$_4$ to 909 cm^{-1} in KTcO$_4$ to 905 cm^{-1} in NaTcO$_4$. The decrease in the stretching frequency is consistent with a slight decrease in the bond strength between Tc and O due to increased interaction between the terminal oxo groups and the alkali cation ongoing from Rb to Na. The simplest explanation is polarization of the oxo electrons away from the Tc center due to electrostatic interaction, which slightly weakens the Tc−O bond.

4.5. NMR. Static and MAS NMR spectra are shown in Figure 6, with the fitting results shown in Table 3. ^{99}Tc is a spin $^9/_2$ quadrupolar nucleus, and its odd oxidation states (7, 5, 3, and 1) have favorable NMR detection sensitivity of 0.375 relative to ^{1}H = 1.000.[54] All spectra are well-resolved and have a good signal-to-noise ratio. Simulations of both the static and MAS NMR spectra, used to extract the quadrupolar coupling constant (C$_q$) and isotropic chemical shift (δ$_{iso}$), agree well with the experimental measurements (Figure 6). Extracted parameters vary slightly between the static and MAS fits. Simulations assumed that η [the asymmetry of the quadrupolar interaction, related to the principal components of the electric-field-gradient (EFG) tensor] was equal to zero for the scheelite structures because of their axial symmetry but not for CsTcO$_4$.

Previous work by Kidd et al.[54] has determined that isolated pertechnetate anions in solutions have relatively low quadrupolar constants (C$_q$), and it was concluded that the structure of an isolated pertechnetate ion solution is a (perfectly) symmetric tetrahedron. Later research by Tarasov and colleagues[14] found that the chemical properties of the solid alkali pertechnetates are strongly dependent on the distortion of this symmetry, with the degree of distortion deceasing as a function of an increase in the countercation radius. Previous NMR assessment of the room temperature form of CsTcO$_4$ determined a C$_q$ of 1.25 MHz, an η of 0.22, and the EFG q$_z$ = 0.35 × 10^{14} esu/cm^3.[14] Tc-99 NMR as a function of the temperature was also reported, and second-order quadrupolar coupling and chemical shift anisotropy were negligible for CsTcO$_4$.[23] A nonzero value of η indicates the absence of axial symmetry at the pertechnetate ^{99}Tc site, and while symmetry is expected in scheelite-type structures, this is not necessarily so in the pseudoscheelite structure.[37] Our results for CsTcO$_4$ are therefore consistent with these previous observations.
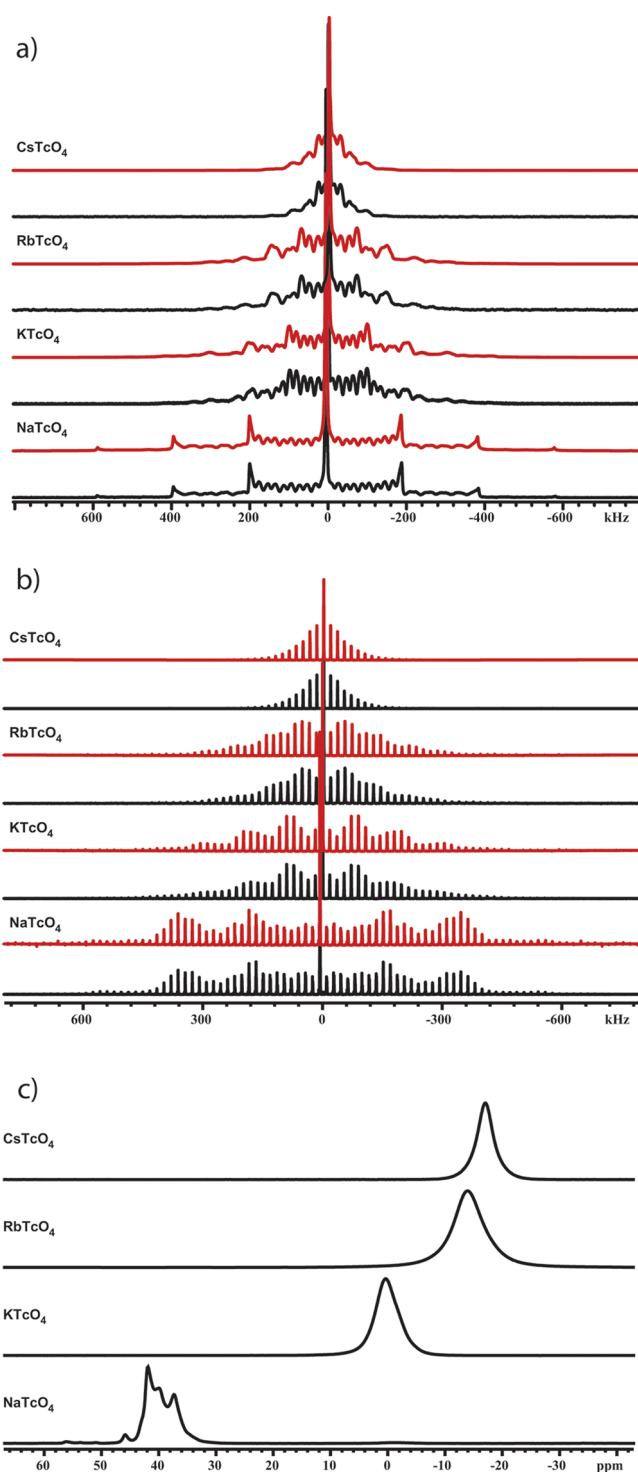

Figure 6. NMR data: (a) static spectra; (b) MAS spectra; (c) central transition of the MAS data. In parts a and b, the top of each pair is the simulated spectrum (red line), while the bottom of each pair is the experiment (black line).

The C$_q$ values decrease as the countercation size increases, with CsTcO$_4$ having the lowest value. It has been suggested previously that the lattice contribution does not explain the high value of the quadrupolar coupling constant in alkali pertechnetates; therefore, the valence electrons must contribute significantly for all scheelite structures.[14] This is consistent with the Na cation having the most tightly bound valence electrons

(the highest first ionization energy) and therefore the largest C_q.

The chemical shifts of the alkali pertechnetates exhibit a change from positive to negative following an increase in the cation size (Na → Cs), which is consistent with the previously published results on sodium, potassium, and rubidium pertechnetates.[14] The largest relative chemical shift difference was found to be between NaTcO$_4$ and KTcO$_4$; subsequent differences between the ppm values for the other compounds were small in comparison. This trend suggests that the electron density around the Tc atoms of NaTcO$_4$ are significantly reduced compared to the Tc atoms of the other alkali pertechnetates and may be a factor in the increased covalency suggested by this compound's Raman spectrum. Of all of the alkalis studied, Na has the highest Pauling electronegativity, leading to electron withdrawal and resultant deshielding of the ^{99}Tc nucleus. This is exactly what is observed, where the δ_{iso} value of sodium pertechnetate is positive with respect to TcO$_4^-$(aq) and deshielded compared to the K, Rb, and Cs compounds, which are negative with respect to TcO$_4^-$(aq). The distinguishable change in the chemical shift values for the alkali pertechnetates suggests that solid-state NMR can be used to identify the presence of a specific, crystalline alkali pertechnetate compound in a solid if it is present in appreciable amounts.

In addition to the chemical shifts, informative data were also collected from the dipolar and quadrupolar interactions between the Tc and its surrounding environment. All anisotropic first-order dipolar and quadrupolar interactions are suppressed with MAS, but second-order quadrupolar interactions are not averaged to zero. Because the outer transitions of the quadrupoles are also excited with the RF pulse, a manifold of spinning sidebands is present and separated at intervals equal to the spinning rate of 18 kHz (Figure 6b). Additionally, the central transition of NaTcO$_4$ has the only quadrupolar coupling large enough that the residual line shape is still visible at this magnetic field strength and spinning speed (Figure 6c). The small peak at 46 ppm arises from the outer transitions (verified by line-shape simulations); however, deviation of the central transition from an ideal line shape (feature in the center at 40 ppm) has not been explained yet. Self-irradiation of an older sample could cause perceptible changes, as could small impurities. However, different Tc sites may be resolvable for NaTcO$_4$, assuming that the local Tc symmetry is quite distorted from tetrahedral. It was also observed that the number of these resonances varied with the spinning speed (see Figure S-9).

4.6. Discussion. *4.6.1. Unexpected Aspects of NaTcO$_4$.* There are several aspects of the data set collected on NaTcO$_4$ that distinguish it from the other alkali pertechnetates. The ND results and quadrupolar coupling show that the TcO$_4^-$ anion has the most distortion from ideal tetrahedral geometry in this compound. The vibrational frequency shift of NaTcO$_4$ and the ^{99}Tc chemical shift suggest either greater covalency or larger polarization due to the interactions between Na$^+$ and the pertechnetate anion. The relative intensity increase of the s/p transitions from XANES analysis suggests an increased interaction between the excited photoelectron and those orbitals. Additionally, this material is more difficult to prepare, and it required more time (approximately an additional 3 h) to dry to a constant weight compared to the other alkali pertechnetates. When the material was exposed to a moist atmosphere for more than 1 h, its weight increased, most likely

because of the adsorption of atmospheric water onto its surface. No evidence for structural water modes of ~3000 cm^{-1} was seen in any samples including NaTcO$_4$, so apparently this is not the hydrated form of sodium pertechnetate. These differences can most likely be attributed to the smaller size of the Na cation and how it fits into the scheelite structure. The calculated cell volume of NaTcO$_4$ is ~339 Å^3, which is ~72 or ~111 Å^3 smaller than the cell volume of KTcO$_4$ and RbTcO$_4$, respectively. As shown in Figure 7, a difference in the unit cell volume is not entirely due to the different sizes of the countercation, although the trend is quite linear. In addition, the O–Tc–O bond angles are different for the Na compound compared to those of K and Rb. These slight changes may be explained by the short alkali–O bond length, which, in turn, because of electrostatics, distorts the TcO$_4^-$ anion. A similar
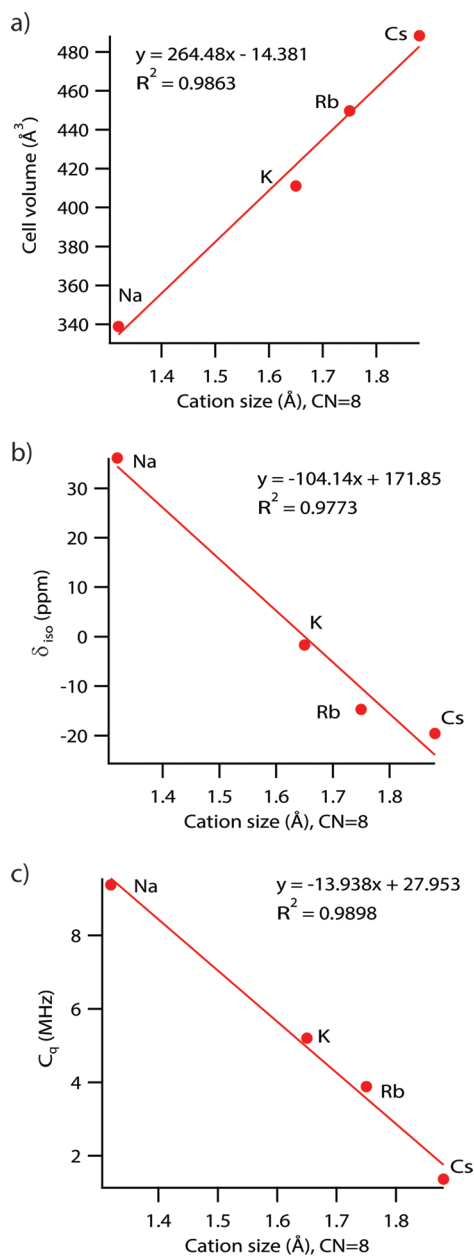

Figure 7. Trends for the alkali pertechnetates by the radius of the alkali: (a) cell volume; (b) δ_{iso} from the fit of static NMR; (c) C_q from the fit of static NMR.

phenomenon has been observed for AgTcO$_4$, which shows short Ag−O bonds and two widely differing O−Tc−O angles.[55] Figure 7 shows the plotted trends in the cell volume, quadrupolar coupling constant, and isotropic chemical shift versus the ionic radius ["CR" value for coordination number (CN) = 8 of alkali[56]].

4.6.2. Lithium Pertechnetates, Lithium Perrhenates, and Hydrated Forms. Lithium pertechnetate was not included in this study because it primarily crystallizes as a hydrated salt, whereas the other alkali pertechnetates generally crystallize as dehydrated salts, with the possible exception of NaTcO$_4$·4H$_2$O. This hydrated sodium pertechnetate, whose X-ray pattern was described in German et al.,[57] has been reported to dehydrate to the scheelite structure NaTcO$_4$ and, upon further heating, to convert to two additional uncharacterized dehydrated structures.[58] Similarly, the dehydrated and hydrated forms of the lithium pertechnetate compounds are thought to be crystal structures distinctly different from the other alkali pertechnetates, although the structures are less well-known than the scheelite structures. As has been pointed out elsewhere,[59] the structure and symmetry of the pertechnetate ion is strongly dependent on not only the cation but also the crystal structure.

LiTcO$_4$ was proposed by Keller and Kanellakopulos[60] to be isostructural to LiReO$_4$. The perrhenate compound has reported hydrated and dehydrated forms, with the number of water molecules per formula unit equaling 0 (refs 61 and 62; space group $P\bar{1}$ per Betz and Hoppe[62]), 1 (refs 61 and 63; space group $P2_1/a$ per Abakumov et al.[63]), 1.5 (refs 63−65; space group $P2_1/c$ per Khrustalev et al.[64]), and 2 (refs 61 and 66; space group not determined). In the Tc system, crystals with water molecules per formula unit have been reported as 0 (refs 14, 60, and 67; reportedly isostructural with LiReO$_4$), 2 (ref 66; reportedly isostructural with LiReO$_4$·2H$_2$O), and 3 (space group $P6_3/mc$ according to Maruk et al.[68]).

Maruk et al.[68] has shown that a trihydrate species of lithium pertechnetates can be synthesized with the careful addition of water to a concentrated solution of lithium pertechnetate and subsequent drying over a strong desiccant for 6 months. According to the literature, lithium pertechnetate dihydrate would be the expected structure of the lithium−technetium oxide compound formed if synthesized using the methods discussed in this manuscript, although this has yet to be experimentally proven and is a focus of future research. For the purposes of comparison for the current study, only scheelite and the related pseudoscheelite structure were of interest because the consideration of multiple hydrations and multiple other crystal structures is a considerable complication.

4.6.3. Relationship between the Scheelite and Pseudo-scheelite Structures. RbTcO$_4$ is a scheelite structure, and related scheelite structures are RbIO$_4$[69] and RbReO$_4$[35,70] but not RbMnO$_4$, which has space group *Pnma*.[69] It has been shown that there are pressure-induced phase transitions of RbReO$_4$ (∼1.6 GPa) and KReO$_4$ (∼7.5 GPa) to an orthorhombic pseudoscheelite-type structure, presumably with space group *Pnma* analogous to CsReO$_4$.[71] One could argue then that the orthorhombic room temperature phase of CsReO$_4$ (and presumably CsTcO$_4$) is a result of "chemical pressure". The only known room temperature orthorhombic pertechnetates are CsTcO$_4$ and TlTcO$_4$,[60] which have corresponding high-temperature tetragonal structures.[43] All of the other alkali pertechnetates (except Li), including Ag$^+$ and NH$_4^+$, have tetragonal structures.[60] The large ion sizes of Cs

and Tl result in chemical pressure to convert to the lower-symmetry form.

It has been shown that the stable structure for ABO$_4$ compounds is largely controlled by the ion radius ratios.[72] Performing similar calculations on pertechnetates, perrhenates, periodates, and permanganates shows that the transition from tetragonal to orthorhombic occurs at lower values of the (r_A + r_B)/$2r_O$ ratio for ABO$_4$ when the B ion is smaller for a given A ion (i.e., alkali permanganates have more room temperature orthorhombic structures; see the SI for details of the calculations).

CsReO$_4$ has both a higher-symmetry, tetragonal ($I4_1/amd$) α form at high temperature (above 470 K) and a lower-symmetry, orthorhombic (*Pnma*) β form at room temperature.[52] Room temperature CsBrO$_4$ is thought to be isostructural with α-CsReO$_4$,[73] while room temperature CsIO$_4$[74] and CsMnO$_4$[69] are isostructural with β-CsReO$_4$. Previous ^{99}Tc NMR on CsTcO$_4$ suggests that there is a transition from orthorhombic to tetragonal at ∼440 K.[23] Thus, in these crystal structures, high temperatures favor the tetragonal phase (lower packing density and higher symmetry) and high pressures favor the orthorhombic phase (higher packing density and lower symmetry).

The results collected in this study on CsTcO$_4$ suggest that the low-temperature, wet-chemical synthesis method described above resulted in formation of the pseudoscheelite structure (*Pnma*). This finding is consistent with the fitting of the ND pattern with a CIF based on the pseudoscheelite version of this compound and from the NMR data, where an asymmetry parameter (η_q) is needed to fit the data (Table 4). However,

Table 4. NMR Fitted Parameters, Including the Asymmetry Parameter (η_q) Fixed at 0.0 for All Except CsTcO$_4$

	expt	C_q (MHz)	η_q	δ_{iso} (ppm)
NaTcO$_4$	MAS	9.38	0	43.5
	static	9.38	0	36.1
KTcO$_4$	MAS	5.33	0	1.5
	static	5.20	0	−1.7
RbTcO$_4$	MAS	3.88	0	−13.4
	static	3.88	0	−14.7
CsTcO$_4$	MAS	1.39	0.228	−16.8
	static	1.36	0.213	−19.6

Raman analysis suggests that the material has a vibrational spectrum very similar to that of scheelite. This difference is most likely due to the insensitive nature of Raman to certain vibration bands of the pseudoscheelite structure because the spectrum is dominated by the TcO$_4$ tetrahedron vibrational modes, which only weakly interact with the Cs atoms, as shown by the low C_q.

4.6.4. Relevance of the Results to Understanding the Chemistry of Tc during Nuclear Waste Immobilization. The periodic trends discussed in this study can bring insight to the behavior of Tc during waste immobilization. According to current baseline plans for the disposal of legacy defense waste from Cold War plutonium production in the United States, a significant portion of the ∼1200 kg of ^{99}Tc inventory at the Hanford site in Washington state will be immobilized in high sodium oxide, aluminum borosilicate glasses.[75] Additionally, a recent paper published by Soderquist and co-workers[76] describes the crystallization of Na and K pertechnetate out of a nuclear waste glass surface. Their results suggest that there is a

high concentration of dissolved pertechnetate at the glass surface when it is quenched. Using the data collected in this currently study of alkali pertechnetates as a baseline, it may be possible to model pertechnetate behavior in oxidizing glass melts at elevated temperatures, and develop a mechanism, based on the structural stability described here, that would explain the results presented by Soderquist et al. Along the same line of research, there remains an uncertain connection between the volatility of ^{99}Tc during vitrification and the amount of sulfides and, separately, the amount of Cs in the melt.[77] On the basis of the discussion provided above, a prudent research path may be to look at the stability of $CsTcO_4$ in both of its crystalline forms under waste glass melt conditions.

As more researchers step away from using Re in place of Tc, an understanding of the fundamental chemistry of the most common Tc starting materials, alkali pertechnetates, will be invaluable. This will be particularly important to the development of many next-generation nuclear waste forms and new vitrification starting materials. A number of these innovative materials have only been investigated with analogues Re compounds or are just beginning to be synthesized with Tc.[78,79] Understanding the stability and chemistry of the alkali pertechnetates will be essential to the design and fine-tuning of these materials so they will efficiently and effectively retain Tc in all of its alkali forms.

Finally, in the realm of inorganic chemistry, there are still many solid-state alkali Tc compounds whose chemistries are still not well-defined. Many of these compounds, including peroxide complexes, carbonyl complexes, pertechnic acid, and higher-order alkali technetium oxides, exist in analogues Re, Cr, and/or Mo forms; however, some do not.[80] Many of these materials have structures similar to those described above, and the information provided in this study could aid in their analysis. Future knowledge of these less well-studied compounds could help in completing an understanding of certain trend-breaking chemistries that occur in the d-block of the periodic table. Subsequently, the methods and novel sample analysis procedures detailed here could be used to more safely synthesize and analyze these compounds.

5. SUMMARY AND CONCLUSIONS

Updated high-resolution spectroscopic and diffraction data have been presented on sodium, potassium, rubidium, and cesium pertechnetates that have been produced using low-temperature, wet-chemical methods. The purities and identities of the pertechnetates were established by ND. Both NMR and XAS analyses of the compounds are sensitive to the identity of the countercation and could be used to identify the presence of these compounds, if crystalline and in appreciable quantity, in other solid materials, such as Tc glasses or minerals. $NaTcO_4$ was found to be significantly different from the other scheelite structured alkali pertechnetates. This difference is most likely the result of the small size of the Na cation and its greater electronegativity than the other alkali tested, resulting in an effect on the terminal oxo groups of the TcO_4^- anion. It was also determined that the low-temperature methods used for the synthesis produced the pseudoscheelite form of $CsTcO_4$, and the formation of this orthorhombic structure during low-temperature synthesis is the result of chemical pressure induced by the large Cs cation.

■ ASSOCIATED CONTENT

ⓈSupporting Information

The Supporting Information is available free of charge on the ACS Publications website at DOI: 10.1021/acs.inorgchem.6b02694.

> Raw NMR datafiles (ZIP)
> CIF based on ND data (CIF)
> CIF based on ND data (CIF)
> CIF based on ND data (CIF)
> CIF based on ND data (CIF)
> Crystallographic information files (CIFs) based on ND data, fit details for ND and XAS data, XRD spectra, Raman spectra with indexed peaks, NMR of $NaTcO_4$ versus spinning speed, and ionic radii calculations for pertechnetates/perrhenates/periodates/permanganates (PDF)

■ AUTHOR INFORMATION

Corresponding Author
*E-mail: john.mccloy@wsu.edu. Tel: 509-335-7796.

ORCID ⊙
Nancy M. Washton: 0000-0002-9643-6794
Wayne W. Lukens: 0000-0002-0796-7631
John S. McCloy: 0000-0001-7476-7771

Notes
The authors declare no competing financial interest.

■ REFERENCES

(1) Deutsch, E.; Libson, K.; Jurisson, S.; Lindoy, L. F. In *Progress in Inorganic Chemistry*; Lippard, S. J., Ed.; John Wiley & Sons, Inc.: New York, 1983; pp 75−139.

(2) Spitsin, V. I.; Rosenfeld, I. L.; Persiantseva, V. P.; Zamoshnikova, N. N.; Kuzina, A. F. Investigation of Inhibiting Properties Of the Pertechnetate Ion. *Corrosion* **1965**, *21*, 211–221.

(3) Ishida, T.; Mazaki, H. Superconducting transition of electrodeposited technetium. *Phys. Rev. B: Condens. Matter Mater. Phys.* **1979**, *20*, 131–138.

(4) Little-Marenin, I. R.; Little, S. J. Technetium in late-type stars. I - Observations. *Astron. J.* **1979**, *84*, 1374–1383.

(5) Goriely, S. *Capture Gamma-Ray Spectroscopy and Related Topics*; World Scientific: Singapore, 2013; pp 326–336.

(6) Kemmitt, R. D. W.; Peacock, R. D. *The chemistry of manganese, technetium, and rhenium: Pergamon texts in inorganic chemistry*; Elsevier: New York, 2013.

(7) McCloy, J. S.; Riley, B. J.; Goel, A.; Liezers, M.; Schweiger, M. J.; Rodriguez, C. P.; Hrma, P.; Kim, D.-S.; Lukens, W. W.; Kruger, A. A. Rhenium Solubility in Borosilicate Nuclear Waste Glass: Implications for the Processing and Immobilization of Technetium-99. *Environ. Sci. Technol.* **2012**, *46*, 12616–12622.

(8) Soderquist, C. Z.; Schweiger, M. J.; Kim, D.-S.; Lukens, W. W.; McCloy, J. S. Redox-Dependent Solubility of Technetium in Low Activity Waste Glass. *J. Nucl. Mater.* **2014**, *449*, 173–180.

(9) McKeown, D. A.; Buechele, A. C.; Lukens, W. W.; Shuh, D. K.; Pegg, I. L. Raman studies of technetium in borosilicate waste glass. *Radiochim. Acta* **2007**, *95*, 275–280.

(10) Gassman, P. L.; McCloy, J. S.; Soderquist, C. Z.; Schweiger, M. J. Raman analysis of perrhenate and pertechnetate in alkali salts and borosilicate glasses. *J. Raman Spectrosc.* **2014**, *45*, 139–147.

(11) Bibler, N. E.; Jurgensen, A. R. Leaching Tc-99 from SRP glass in simulated tuff and salt groundwaters. *MRS Online Proc. Libr.* **1987**, *112*, 585–593.

(12) Migge, H. Simultaneous evaporation of cesium and technetium during vitrification - a thermochemical approach. *MRS Online Proc. Libr.* **1989**, *176*, 411–417.

(13) Donald, I. W.; Metcalfe, B. L.; Taylor, R. N. J. The immobilization of high level radioactive wastes using ceramics and glasses. *J. Mater. Sci.* **1997**, *32*, 5851–5887.

(14) Tarasov, V. P.; Petrushin, S. A.; Privalov, V. I.; German, K. E.; Kryuchkov, S. V.; Buslaev, Y. A. Quadrupole nuclear interaction of technetium-99 in polycrystalline pertechnetates. *Koord. Khim.* **1986**, *12*, 1227–1236.

(15) Busey, R. H.; Keller, O. L., Jr. Structure of the aqueous pertechnetate ion by Raman and infrared spectroscopy. Raman and infrared spectra of crystalline $KTcO_4$, $KReO_4$, Na_2MoO_4, Na_2WO_4, $Na_2MoO_4 \cdot 2H_2O$, and $Na_2WO_4 \cdot 2H_2O$. *J. Chem. Phys.* **1964**, *41*, 215–225.

(16) Krebs, B.; Hasse, K.-D. Refinements of the Crystal Structures of $KTcO_4$, $KReO_4$, and OsO_4: Bond lengths in tetrahedral oxo-anions and oxide of d^0 transition metals. *Acta Crystallogr., Sect. B: Struct. Crystallogr. Cryst. Chem.* **1976**, *32*, 1334–1337.

(17) Colton, R.; Peacock, R. D. An outline of technetium chemistry. *Q. Rev., Chem. Soc.* **1962**, *16*, 299–315.

(18) Banerjee, S.; Ambikalmajan Pillai, M. R.; Ramamoorthy, N. Evolution of Tc-99m in diagnostic radiopharmaceuticals. *Semin. Nucl. Med.* **2001**, *31*, 260–277.

(19) German, K. E.; Kryuchkov, S. V.; Belyaeva, L. I. Synthesis of sodium pertechnetate tetrahydrate and its thermal properties. *Izv. Akad. Nauk SSSR, Ser. Khim.* **1988**, *19*, 2387.

(20) Errico, L.; Darriba, G.; Rentería, M.; Tang, Z.; Emmerich, H.; Cottenier, S. Nuclear quadrupole moment of the ^{99}Tc ground state. *Phys. Rev. B: Condens. Matter Mater. Phys.* **2008**, *77*, 195118.

(21) Darab, J. G.; Smith, P. A. Chemistry of Technetium and Rhenium Species during Low-Level Radioactive Waste Vitrification. *Chem. Mater.* **1996**, *8*, 1004–1021.

(22) Meyer, G.; Hoppe, R. The crystal structure of cesium pertechnetate. *Z. Anorg. Allg. Chem.* **1976**, *420*, 40–50.

(23) Tarasov, V. P.; Kirakosyan, G. A.; German, K. E. Anomalous temperature dependence of the technetium-99 quadrupole coupling and disordering of cesium positions in cesium pertechnetate. *Z. Naturforsch., A: Phys. Sci.* **1992**, *47*, 325–329.

(24) Colton, R. *The chemistry of rhenium and technetium*; Interscience Publishers: New York, 1965.

(25) Cotton, A. F.; Wilkinson, G.; Bochmann, M.; Murillo, C. A. *Advanced inorganic chemistry*; Wiley: New York, 1999.

(26) Buechele, A. C.; Lukens, W. W.; Shuh, D. K.; McKeown, D. A.; Muller, I. S.; Pegg, I. L. Comparison of the behavior of technetium and rhenium in low activity waste glass formulations subjected to the vapor hydration test. *Microsc. Microanal.* **2010**, *16*, 1628–1629.

(27) Lukens, W. W.; McKeown, D. A.; Buechele, A. C.; Muller, I. S.; Shuh, D. K.; Pegg, I. L. Dissimilar Behavior of Technetium and Rhenium in Borosilicate Waste Glass as Determined by X-ray Absorption Spectroscopy. *Chem. Mater.* **2007**, *19*, 559–566.

(28) McKeown, D. A.; Buechele, A. C.; Lukens, W. W.; Shuh, D. K.; Pegg, I. L. Tc and Re Behavior in Borosilicate Waste Glass Vapor Hydration Tests. *Environ. Sci. Technol.* **2007**, *41*, 431–436.

(29) Neuefeind, J.; Feygenson, M.; Carruth, J.; Hoffmann, R.; Chipley, K. K. The Nanoscale Ordered MAterials Diffractometer NOMAD at the Spallation Neutron Source SNS. *Nucl. Instrum. Methods Phys. Res., Sect. B* **2012**, *287*, 68–75.

(30) Toby, B. EXPGUI, a graphical user interface for GSAS. *J. Appl. Crystallogr.* **2001**, *34*, 210–213.

(31) Schwochau, K. Die Kristallstruktur von Natrium- und Silberpertechnetat [Crystal structure of $NaTcO_4$ and $AgTcO_4$]. *Z. Naturforsch., A: Phys. Sci.* **1962**, *17*, 630.

(32) Webb, S. M. SIXpack: a graphical user interface for XAS analysis using IFEFFIT. *Phys. Scr.* **2005**, *2005*, 1011–1014.

(33) Ravel, B.; Newville, M. ATHENA, ARTEMIS, HEPHAESTUS: data analysis for X-ray absorption spectroscopy using IFEFFIT. *J. Synchrotron Radiat.* **2005**, *12*, 537–541.

(34) Bak, M.; Rasmussen, J. T.; Nielsen, N. C. SIMPSON. A general simulation program for solid-state NMR spectroscopy. *J. Magn. Reson.* **2000**, *147*, 296–330.

(35) Beintema, J. The crystal structure of the alkali perrhenates and periodates. *Z. Kristallogr. - Cryst. Mater.* **1937**, *97*, 300–322.

(36) McDonald, B. J.; Tyson, G. J. The crystal structures of cesium, ammonium, and potassium pertechnetates. *Acta Crystallogr.* **1962**, *15*, 87.

(37) Spitsyn, V. I.; Tarasov, V. P.; German, K. E.; Petrushin, S. A.; Kuzina, A. F.; Kryuchkov, S. V. Symmetry of d^0-oxo complexes of technetium according to the technetium-99 NMR data. *Dokl. Akad. Nauk SSSR* **1986**, *290*, 1411–1413.

(38) Keller, C.; Kanellakopulos, B. Ternary oxides of tri- to septivalent technetium and alkali metals. *J. Inorg. Nucl. Chem.* **1965**, *27*, 787–795.

(39) Lukens, W. W.; Shuh, D. K.; Muller, I. S.; McKeown, D. A. X-ray Absorption Fine Structure Studies of Speciation of Technetium in Borosilicate Glasses. *MRS Online Proc. Libr.* **2003**, *802*, DD3.3.1–DD3.3.6.

(40) Mikkelsen, J. C.; Boyce, J. B. Extended-x-ray-absorption-fine-structure study of $Ga_{2/3}Se$ polymorphs and $GaAs$-$Ga_{2/3}Se$ solid solutions. *Phys. Rev. B: Condens. Matter Mater. Phys.* **1981**, *24*, 5999–6009.

(41) Mikkelsen, J. C.; Boyce, J. B. Extended x-ray-absorption fine-structure study of $Ga_{1-x}In_xAs$ random solid solutions. *Phys. Rev. B: Condens. Matter Mater. Phys.* **1983**, *28*, 7130–7140.

(42) Kanellakopulos, B. *The ternary oxide of 3-to 7-valent technetium with alkalis*; IssueAEC Accession No. 31424, Report No. KFK-197; Kernforschungszentrum Institute of Radiochemistry: Karlsruhe, Germany, 1964.

(43) Kanellakopulos, B. Zur kenntnis der hochtemperaturmodifikation einiger verbindungen des typs Me^IXO_4 (Me = Cs, Tl; X = Re, Tc, Cl) [High temperature modification of some compounds of the type MXO_4 (M(I) = cesium, thallium; X = rhenium, technetium, chlorine)]. *J. Inorg. Nucl. Chem.* **1966**, *28*, 813–816.

(44) Chandrabhas, N.; Victor, D.; Muthu, S.; Sood, A. K.; Bhat, H. L.; Jayaraman, A. Raman study of pressure-induced structural transitions in cesium periodate ($CsIO_4$) to 12 GPa. *J. Phys. Chem. Solids* **1992**, *53*, 959–965.

(45) Al-Dhahir, T. A.; Sood, A. K.; Bhat, H. L. Incommensurate-commensurate phase transition in ferroelastic CsIO$_4$. *Solid State Commun.* **1989**, *70*, 863−868.

(46) Arthers, S. A.; Beattie, I. R.; Gomme, R. A.; Jones, P. J.; Ogden, J. S. Matrix isolation studies on alkali metal perrhenates: the shape and vibrational assignments of cesium perrhenate, CsReO$_4$. *J. Chem. Soc., Dalton Trans.* **1983**, 1461−1464.

(47) Müller, A.; Rittner, W. I.R.-Spektren der Pertechnetate und Perrhenate des Tetrabutylammoniums und Tetraphenylarsoniums und Faktorgruppenanalyse der Optischen Schwingungen von KTcO$_4$ im I.R.- und Ramanspektrum. *Spectrochim. Acta, Part A* **1967**, *23*, 1831−1837.

(48) Johnson, R. A.; Rogers, M. T.; Leroi, G. E. Vibrational Spectra of Ammonium and Other Scheelite-Type Perrhenates. *J. Chem. Phys.* **1972**, *56*, 789−792.

(49) Baluka, M.; Hanuka, J. Jezowska-Trzebiatowska. Infrared and Electronic Spectra of the Technetium Oxy-compounds. *B. Acad. Polym. Sci.-Chim.* **1972**, *20*, 271−278.

(50) Korppi-Tommola, J.; Devarajan, V.; Brown, R. J. C.; Shurvell, H. F. The temperature dependence of the Raman spectrum of ammonium perrhenate. *J. Raman Spectrosc.* **1978**, *7*, 96−100.

(51) Ulbricht, K.; Kriegsmann, H. Spektroskopische Untersuchungen an einigen wasserfreien Perrhenaten. *Z. Anorg. Allg. Chem.* **1968**, *358*, 193−209.

(52) Range, K. J.; Roegner, P.; Heyns, A. M.; Prinsloo, L. C. An x-ray, Raman and IR study of α-CsReO$_4$, the high-temperature modification of cesium perrhenate. *Z. Naturforsch., B: Chem. Sci.* **1992**, *47*, 1513−1520.

(53) Petrov, K. I.; Kuzina, A. F.; Dolgorukova, N. I.; Golovin, Y. M.; Spitsyn, V. I. Vibrational spectra of alkali metal and ammonium pertechnetates. *Dokl. Akad. Nauk SSSR* **1972**, *206*, 909−912.

(54) Kidd, R. G. Technetium-99 NMR and rationalized quadrupole moment values for transition metal nuclei. *J. Magn. Reson.* **1981**, *45*, 88−93.

(55) Sarsfield, M. J.; Sutton, A. D.; Livens, F. R.; May, I.; Taylor, R. J. Raman spectroscopy of silver pertechnetate. *Acta Crystallogr., Sect. C: Cryst. Struct. Commun.* **2003**, *59*, i45−i46.

(56) Shannon, R. D. Revised effective ionic radii and systematic studies of interatomic distances in halides and chalcogenides. *Acta Crystallogr., Sect. A: Cryst. Phys., Diffr., Theor. Gen. Crystallogr.* **1976**, *32*, 751−767.

(57) German, K. E.; Grushevschkaya, L. N.; Kryutchkov, S. V.; Pustovalov, V. A.; Obruchikov, V. V. Investigation of Phase Transitions and Other Physico-Chemical Properties of Pertechnetates and Perrhenates of Alkali and Organic Cations. *Radiochim. Acta* **1993**, *63*, 221−224.

(58) German, K. E.; Kryuchkov, S. V.; Belyaeva, L. I. Synthesis of sodium pertechnetate tetrahydrate and its thermal properties. *Izv. Akad. Nauk SSSR, Ser. Khim.* **1987**, *10*, 2387.

(59) Kryutchkov, S. V.; Grigoriev, M. S.; German, K. E. In *Technetium and Rhenium in chemistry and nuclear medicine*; Nicolini, M., Bandoly, G.; Mazzi, U., Eds.; Cortina International: Verona, Padova, Italy, 1990; pp 253−264.

(60) Keller, C.; Kanellakopulos, B. Preparation and investigation of some pertechnetates of the type M^{I}TcO$_4$. *Radiochim. Acta* **1963**, *1*, 107−108.

(61) Smith, W. T.; Long, S. H. The Salts of Perrhenic Acid. I. The Alkali Metals and Ammonium. *J. Am. Chem. Soc.* **1948**, *70*, 354−356.

(62) Betz, T.; Hoppe, R. Über Perrhenate. 1. Zur Kenntnis von LiReO$_4$. *Z. Anorg. Allg. Chem.* **1983**, *500*, 23−30.

(63) Abakumov, A. M.; Rozova, M. G.; Shpanchenko, R. V.; Mironov, A. V.; Antipov, E. V.; Bramnik, K. G. Synthesis and crystal structure of the lithium perrhenate monohydrate LiReO$_4$·H$_2$O. *Solid State Sci.* **2001**, *3*, 581−586.

(64) Khrustalev, V. N.; Varfolomeev, M. B.; Shamrai, N. B.; Lindeman, S. V.; Struchkov, Y. T. Crystal structure of lithium perrhenate sesquihydrate. *Zh. Neorg. Khim.* **1995**, *26*, 208−213.

(65) Scholder, R.; Huppert, K. L. Alkali and alkaline earth oxorhenates(VII). *Z. Anorg. Allg. Chem.* **1964**, *334*, 209−224.

(66) Zaitseva, L. L.; Konarev, M. I.; Velichko, A. V. Lithium pertechnetate and perrhenate. *Zh. Neorg. Khim.* **1977**, *22*, 2348−2353.

(67) Vida, J. *The chemical behavior of technetium during treatment of high-level radioactive waste [translated from German by J. R. Jewett]*, PNL-TR-497; Battelle Pacific Northwest Laboratory: Richland, WA, 1994.

(68) Maruk, A. Y.; Grigor'ev, M. S.; German, K. E. Lithium pertechnetate trihydrate LiTcO$_4$·3H$_2$O: Synthesis and crystal structure. *Russ. J. Coord. Chem.* **2011**, *37*, 444−446.

(69) Hoppe, R.; Fischer, D.; Schneider, J. Zur Kenntnis von Oxyden A[MO$_4$]: Über LiMnO$_4$, KMnO$_4$, RbMnO$_4$, CsMnO$_4$ sowie RbIO$_4$ und CsIO$_4$. (− Was heißt eigentlich "Die Kristallstruktur von···"? −). *Z. Anorg. Allg. Chem.* **1999**, *625*, 1135−1142.

(70) Ulbricht, K.; Kriegsmann, H. Die Raman-Spekren einiger wasserfreier Perrhenate [Raman spectra of certain anhydrous perrhenates]. *Z. Chem.* **1966**, *6*, 232−233.

(71) Jayaraman, A.; Kourouklis, G. A.; Van Uitert, L. G.; Grodkiewicz, W. H.; Maines, R. G. A high-pressure Raman study of potassium perrhenate, rubidium perrhenate, and cesium perrhenate to 25 GPa and pressure-induced phase transitions. *Phys. A* **1989**, *156*, 325−340.

(72) Fukunaga, O.; Yamaoka, S. Phase transformations in ABO$_4$ type compounds under high pressure. *Phys. Chem. Miner.* **1979**, *5*, 167−177.

(73) Rögner, P.; Schießl, U.; Range, K.-J. On the Space Group of Cesium Perbromate, CsBrO$_4$. *Z. Naturforsch., B: J. Chem. Sci.* **1993**, *48*, 235−236.

(74) de Waal, D.; Zabel, M.; Range, K.-J. The Crystal Structure of β-CsIO$_4$, the Room-Temperature Modification of Cesium Periodate. *Z. Naturforsch., B: J. Chem. Sci.* **1996**, *51*, 441−443.

(75) Kruger, A. A.; Kim, D. S. Technetium Incorporation in Glass for the Hanford Tank Waste Treatment and Immobilization Plant, Hanford Site (HNF), Richland, WA, 2015.

(76) Soderquist, C. Z.; Buck, E. C.; McCloy, J. S.; Schweiger, M. J.; Kruger, A. A. Formation of Technetium Salts in Hanford Low Activity Waste Glass. *J. Am. Ceram. Soc.* **2016**, *99*, 3924−3931.

(77) Migge, H. Simultaneous evaporation of cesium and technetium during vitrification—a thermochemical approach. *Mater. Res. Soc. Symp. Proc.* **1989**, *176*, 411−417.

(78) Luksic, S. A.; Riley, B. J.; Parker, K. E.; Hrma, P. Sodalite as a vehicle to increase Re retention in waste glass simulant during vitrification. *J. Nucl. Mater.* **2016**, *479*, 331−337.

(79) Lee, M.-S.; Um, W.; Wang, G.; Kruger, A. A.; Lukens, W. W.; Rousseau, R.; Glezakou, V.-A. Impeding ^{99}Tc(IV) mobility in novel waste forms. *Nat. Commun.* **2016**, *7*, 12067.

(80) Schwochau, K. *Technetium: Chemistry and Radiopharmaceutical Applications*; Wiley: New York, 2000.

(81) Boyd, G. E. Technetium and promethium. *J. Chem. Educ.* **1959**, *36*, 3−14.

(82) Tarasov, V. P.; Kirakosyan, G. A.; German, K. E. Anomalous temperature dependence of quadrupole coupling constant of technetium-99 and disordering of cesium ions in cesium pertechnetate lattice. *Z. Naturforsch., A: Phys. Sci.* **1992**, *47*, 1643−1653.